INTERNATIONAL JOURNAL FOR NUMERICAL METHODS IN FLUIDS
Int. J. Numer. Meth. Fluids **28**: 477–499 (1998)

NATURAL CONVECTION IN PARTIALLY COOLED TILTED CAVITIES

M.M. EL-REFAEE, M.M. ELSAYED, N.M. AL-NAJEM* AND A.A. NOOR

Mechanical and Industrial Engineering Department, Kuwait University, PO Box 5969 Safat 13060, Kuwait

SUMMARY

Two-dimensional numerical simulations of laminar natural convection in a partially cooled, differentially heated inclined cavities are performed. One of the cavity walls is entirely heated to a uniformly high temperature (heat source) while the opposite wall is partially cooled to a lower temperature (heat sink). The remaining walls are adiabatic. The tilt angle of the cavity is varied from 0° (heated from left) to −90° (heated from top). The fast false implicit transient scheme (FITS) algorithm, developed earlier by the same authors, is modified to solve the derived variables vorticity-streamfunction formulation. The effects of aspect ratio (AR), sink–source ratio and tilt angle on the average Nusselt number are examined through a parametric study; solutions are obtained for two Grashof numbers, 10^5 and 10^7. Flow patterns and isotherms are used to investigate the heat transfer and fluid flow mechanisms inside the cavity.

KEY WORDS: natural convection; tilted cavity; partial cooling; storage tanks

1. INTRODUCTION

Natural convection in rectangular cavities has numerous engineering applications, among which are electronic packages, solar collectors, thermal design of buildings, storage systems, cooling of nuclear reactors, etc. Ostrach [1] comprehensively reviewed this subject. Most of the early work dealt with differentially heated vertical cavities where one vertical side is at a high isothermal temperature and the opposite side is at a low isothermal temperature. The remaining sides of the cavity are adiabatic. Several investigators, e.g. Krane and Jessee [2], Barakos *et al.* [3], Markatos and Pericleous [4] and Henkes *et al.* [5] have studied this cavity type.

A subdivision of the natural convection problem in a rectangular cavity is the case where one wall is partially/fully heated and the opposite wall is partially/fully cooled while the other two walls are kept adiabatic. This cavity configuration is of special interest in many engineering applications, such as solar receivers, solar passive design, and cooling of electronic equipment. Table I summarizes some of the work available in the literature for this type of configuration. These types are characterized by the boundary conditions imposed on the walls, as presented in Table II and Figure 1. Only Oosthuizen and Paul [6] studied the effect of the cavity tilt angle, while other studies dealt with a vertical cavity. Hasnaoui *et al.* [7] studied natural convection in a horizontal cavity partially heated from below ($\alpha = 90°$). All the cases

* Correspondence to: Mechanical and Industrial Engineering Department, Kuwait University, PO Box 5969, Safat 13060, Kuwait.

CCC 0271–2091/98/130477–23$17.50

Received March 1997
Revised September 1997

Table I. Review of previous work on rectangular cavities where one wall is fully/partially heated and the opposing wall is fully/partially cooled (see Figure 1)

Reference		H/B	c_1/H	a_1/H	c_2/H	a_2/H	Type*	Tilt α (°)	Ra
Kuhn and Oosthuizen [17]	1987	1	$0.07 \rightarrow 0.7$	$0.1 \rightarrow 0.33$	0.5	1	A	0	$0 \leq Ra_B \leq 10^5$
Oosthuizen and Paul [6]	1989	1	0.5	$0.25 \rightarrow 1.0$	$0.5 \rightarrow 0.63$	1	A	$-90 \rightarrow 90$	$10^3 \leq Ra_B < 10^5$
Hasnaoui *et al.* [7]	1992	1, 2	$0.06 \rightarrow 1.0$	$0.2 \rightarrow 0.85$	0.5	1	A	90	$0 \leq Ra_B \leq 5 \times 10^6$
Oosthuizen and Paul [18]	1991	1	$0.25 \rightarrow 0.75$	$0.25 \rightarrow 0.75$	0.5	1	B	$-90 \rightarrow 90$	$3 \times 10^3 \leq Ra_H \leq 10^5$
Keyhani *et al.* [19]	1988	16.5	R1	R1	0.5	1	C	0	$6.4 \times 10^5 \leq Ra_B \leq 5.3 \times 10^6$
Hadim and Ramot [20]	1993	1	$0.1 \rightarrow 0.9$	0.2	$0.1 \rightarrow 0.9$	0.2	D	0	$0 \leq Ra_B \leq 10^5$
Turner and Flack [8]	1980	$0.5 \rightarrow 2.0$	0.5	1	$1/8 \rightarrow 1/7$	$1/8 \rightarrow 7/8$	E	0	$5 \times 10^6 \leq Ra_H \leq 9 \times 10^6$
Present work		4, 2, 1.33 ,1	0.5	1	0.5	0.2, 0.6, 1.0	E	$-90 \rightarrow 0$	$Gr_B = 10^5,\ 10^7$

* See Table II.

shown in Table I considered the fully cooled wall with partially heated wall, except Turner and Flack [8] who studied a fully heated, partially cooled cavity (type E). The effect of the height and position of the heated portion of the wall on the flow pattern and heat transfer inside the cavity has been studied for cavities with aspect ratios between 0.3 and 16.5, and with Rayleigh numbers of $\leq 10^7$. The investigators listed in Table I found a significant reduction in heat transfer rate for the vertical cavity (i.e. $\alpha = 0°$), when the heated portion of the wall moves away from the wall's center. On the contrary, tilting the cavity in a positive direction (counterclockwise) significantly increases the heat transfer rate. Turner and Flack [8] have predicted the same effect for a fully heated, partially cooled vertical cavity. The rate of heat transfer is reduced as the cooled portion moves either upwards (towards the top wall) or downwards (towards the bottom wall).

In the present work, a numerical parametric study of natural convection inside a fully heated, partially cooled tilted cavity is reported. This problem is of fundamental relevance in designing solar receivers and nuclear reactor cooling systems. Further applications include determining thermal losses in shop refrigerators. The fast false implicit transient scheme (FITS) as described by El-Refaee *et al.* [9] is modified to solve the 2D derived variables governing equations. Solutions are obtained for a range of values of the cavity aspect ratio ($1 \leq AR \leq 4$), sink–source ratio ($1/4 < SR < 1$) and tilting angle ($-90° \leq \alpha \leq 0°$) at Rayleigh numbers $Ra = 10^5$ and 10^7. The sink portion is centered at the cooled wall in the present study. In order to examine the mechanisms of heat and fluid flow inside the cavity, detailed temperature and flow contours are presented. Figure 2 and Table I present the cavity configuration and the parametric range of study, respectively.

2. FORMULATION

The governing conservation equations for two-dimensional natural convection flow inside the cavity shown in Figure 2 are

$$\frac{\partial u}{\partial x} + \frac{\partial v}{\partial y} = 0, \tag{1}$$

$$\frac{\partial u}{\partial t} + u\frac{\partial u}{\partial x} + v\frac{\partial u}{\partial y} = \frac{-1}{\rho_0}\frac{\partial p}{\partial x} + g\beta(T - T_C)\sin\alpha + \upsilon\left(\frac{\partial^2 u}{\partial x^2} + \frac{\partial^2 u}{\partial y^2}\right), \tag{2}$$

Table II. Boundary conditions for different cavity types (see Figure 1)

Type	Boundary conditions on walls							
	1	1A	1B	2	2A	2B	3	4
A	T_H	a	a	T_C	NA	NA	a	a
B	T_H	a	a	a	NA	NA	T_C	a
C	P	P	P	T_C	NA	NA	a	a
D	T_H	a	a	T_H	T_C	T_C	a	a
E	T_H	NA	NA	T_C	a	a	a	a

a, adiabatic.
NA, not applicable (the length of the wall diminishes to zero).
P, walls 1, 1A, 1B are divided into isothermal parts at T_H and adiabatic parts.

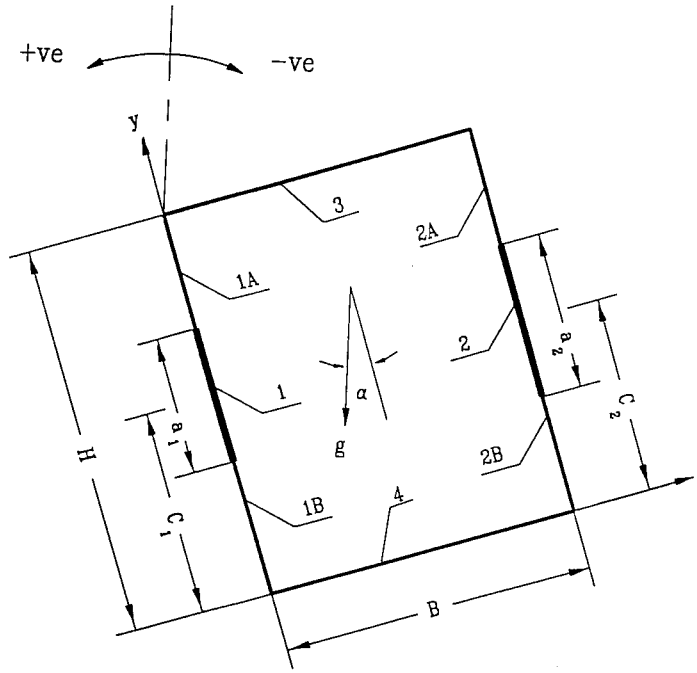

Figure 1. General geometry of a partially heated/cooled tilted cavity.

$$\frac{\partial v}{\partial t}+u\frac{\partial v}{\partial x}+v\frac{\partial v}{\partial y}=\frac{-1}{\rho_0}\frac{\partial p}{\partial y}+g\beta(T-T_C)\cos\alpha+\upsilon\left(\frac{\partial^2 v}{\partial x^2}+\frac{\partial^2 v}{\partial y^2}\right), \tag{3}$$

$$\frac{\partial T}{\partial t}+u\frac{\partial T}{\partial x}+v\frac{\partial T}{\partial y}=\frac{k}{\rho_0 c_p}\left(\frac{\partial^2 T}{\partial x^2}+\frac{\partial^2 T}{\partial y^2}\right), \tag{4}$$

where x and y are Cartesian co-ordinates, u and v are the velocity components in these directions, p is the pressure, T is the temperature and t is the time. The properties ρ, υ, k, c_p and β are assumed to be constant, except for the density variation which is considered only in the buoyancy force through Buosinesque approximation.

Using the streamfunction vorticity formulation, Equations (1)–(4) are reduced to the following

$$\omega=-\left(\frac{\partial^2\psi}{\partial x^2}+\frac{\partial^2\psi}{\partial y^2}\right), \tag{5}$$

$$\frac{\partial\omega}{\partial t}+u\frac{\partial\omega}{\partial x}+v\frac{\partial\omega}{\partial y}=+g\beta\frac{\partial T}{\partial x}\cos\alpha-\frac{\partial T}{\partial y}\sin\alpha+\upsilon\left(\frac{\partial^2\omega}{\partial x^2}+\frac{\partial^2\omega}{\partial y^2}\right), \tag{6}$$

$$\frac{\partial T}{\partial t}+u\frac{\partial T}{\partial x}+v\frac{\partial T}{\partial y^2}=\frac{k}{\rho_0 c_p}\left(\frac{\partial^2 T}{\partial x^2}+\frac{\partial^2 T}{\partial y^2}\right). \tag{7}$$

Introducing the following dimensionless quantities

$$\left.\begin{aligned} X &= \frac{x}{H}, & Y &= \frac{y}{H} \\ U &= \frac{u}{\sqrt{g\beta(T_H - T_C)H}}, & V &= \frac{v}{\sqrt{g\beta(T_H - T_C)H}} \\ \theta &= \frac{T - T_C}{T_H - T_C}, & \tau &= \frac{t\sqrt{g\beta(T_H - T_C)H}}{H} \\ \Psi &= \frac{\psi}{H\sqrt{g\beta(T_H - T_C)H}}, & \Omega &= \frac{\omega H}{\sqrt{g\beta(T_H - T_C)H}} \end{aligned}\right\}, \tag{8}$$

the dimensionless governing equations become

$$\Omega = -\left(\frac{\partial^2\Psi}{\partial X^2} + \frac{\partial^2\Psi}{\partial Y^2}\right), \tag{9}$$

$$\frac{\partial\Omega}{\partial\tau} + U\frac{\partial\Omega}{\partial X} + V\frac{\partial\Omega}{\partial Y} = \left(\frac{\partial\theta}{\partial X}\cos\alpha - \frac{\partial\theta}{\partial Y}\sin\alpha\right) + \frac{1}{\sqrt{Gr}}\left(\frac{\partial^2\Omega}{\partial X^2} + \frac{\partial^2\Omega}{\partial Y^2}\right), \tag{10}$$

$$\frac{\partial\theta}{\partial\tau} + U\frac{\partial\theta}{\partial X} + V\frac{\partial\theta}{\partial Y} = \frac{1}{Pr\sqrt{Gr}}\left(\frac{\partial^2\theta}{\partial X^2} + \frac{\partial^2\theta}{\partial Y^2}\right), \tag{11}$$

$$Pr = \frac{\rho_0 \upsilon c_p}{k}, \qquad Gr = \frac{g\beta(T_H - T_c)H^3}{\upsilon^2}. \tag{12}$$

The vorticity and energy transport equations may now be rewritten in the following general form

$$\frac{\partial\phi}{\partial\tau} + U\frac{\partial\phi}{\partial X} + V\frac{\partial\phi}{\partial Y} = \Gamma_\phi\left(\frac{\partial^2\phi}{\partial X^2} + \frac{\partial^2\phi}{\partial Y^2}\right) + S_\phi, \tag{13}$$

where ϕ stands for Ω or θ, and Γ_ϕ and S_ϕ are as follows

$$\left.\begin{aligned} \Gamma_\Omega &= \frac{1}{\sqrt{Gr}}, & S_\Omega &= \left(\frac{\partial\theta}{\partial X}\cos\alpha - \frac{\partial\theta}{\partial Y}\sin\alpha\right) \\ \Gamma_\theta &= \frac{1}{Pr\sqrt{Gr}}, & S_\theta &= 0 \end{aligned}\right\}. \tag{14}$$

2.1. The discretization of equations

The above governing equations are uniformly discretized using the control volume approach. The power law is employed in discretizing the convection and diffusion terms as described by Patankar [10]. To accelerate the convergence an alternating direction implicit (ADI) scheme is applied [11]. Allowing the power law (almost exact solution) application locally in a one-dimensional sense for each sweep in the co-ordinates directions, the ADI procedure enhances the accuracy of the solution. The resultant discretization equations for Equation (13) in the x- and y-directions are, respectively, as follows

$$-a^{n+1/2}_{i-1,j}\phi^{n+1/2}_{i-1,j} + a^{n+1/2}_{i,j}\phi^{n+1/2}_{i,j} - a^{n+1/2}_{i+1,j}\phi^{n+1/2}_{i+1,j} = b^n, \tag{15}$$

$$-a^{n+1}_{i,j-1}\phi^{n+1}_{i,j-1}+a^{n+1}_{i,j}\phi^{n+1}_{i,j}-a^{n+1}_{i,j+1}\phi^{n+1}_{i,j+1}=b^{n+1/2}, \tag{16}$$

where the subscripts i and j refer to the x- and y-locations of the grid point respectively, and the superscripts n, $n+1/2$, $n+1$ indicate old time, advancing a half time step and advancing a full time step, respectively. The coefficients of Equations (15) and (16) are expressed as follows

$$\left.\begin{aligned}
a^{n+1/2}_{i-1,j} &= \frac{\Delta\tau\Gamma}{\Delta X^2}A(|P^{n+1/2}_{i-1/2,j}|)+\frac{\Delta\tau}{\Delta X}[[U^{n+1/2}_{i-1/2,j},0]]\\
a^{n+1/2}_{i+1,j} &= \frac{\Delta\tau\Gamma_\phi}{\Delta X^2}A(|P^{n+1/2}_{i+1/2,j}|)+\frac{\Delta\tau}{\Delta X}[[-U^{n+1/2}_{i+1/2,j},0]]\\
a^{n+1/2}_{i,j} &= 2+a^{n+1/2}_{i-1,j}+a^{n+1/2}_{i+1,j}\\
b^n &= 2\phi^n_{i,j}+\frac{\Delta\tau\Gamma_\phi}{\Delta Y^2}\{A(|P^n_{i,j+1/2}|)\cdot(\phi^n_{i,j+1}-\phi^n_{i,j})+A(|P^n_{i,j-1/2}|)\cdot(\phi^n_{i,j-1}-\phi^n_{i,j})\}\\
&\quad+\frac{\Delta\tau}{\Delta Y}\{[[-V^n_{i,j+1/2},0]](\phi^n_{i,j+1}-\phi^n_{i,j})+[[V^n_{i,j-1/2},0]](\phi^n_{i,j-1}-\phi^n_{i,j})\}+\Delta\tau\cdot S^n_\phi
\end{aligned}\right\}, \tag{17a}$$

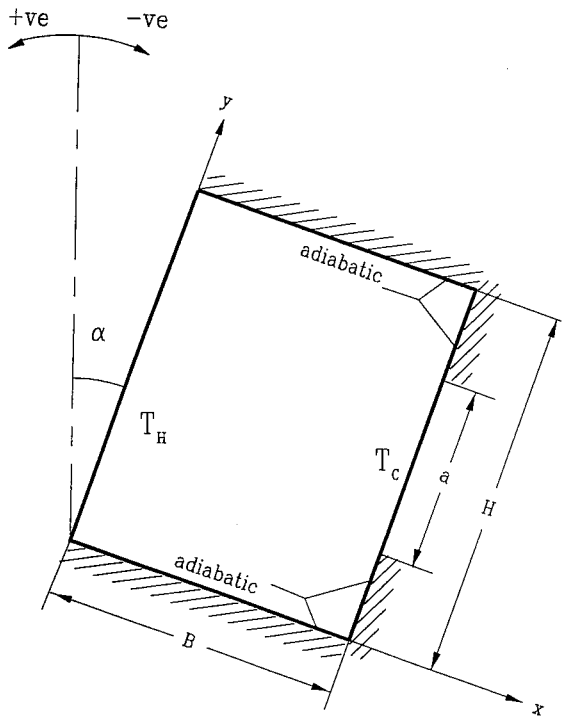

Figure 2. Geometry and dimension of the partially cooled tilted cavity.

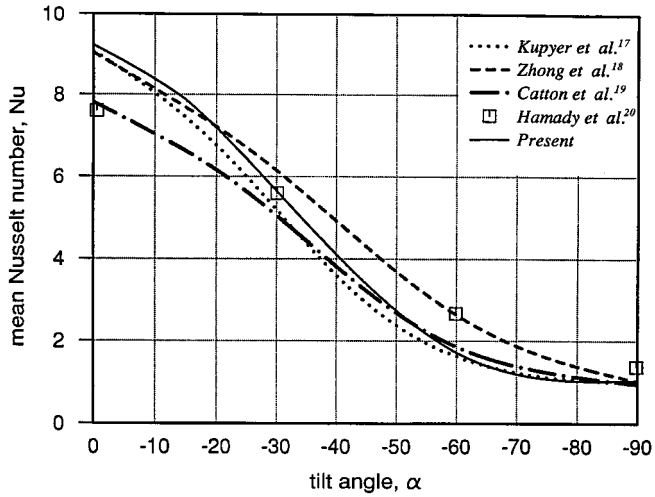

Figure 3. Dependence of mean Nusselt number on tilt angle for $Ra = 10^6$; comparison with other solutions and experimental data.

$$\left.\begin{aligned}
a_{i,j-1}^{n+1} &= \frac{\Delta\tau\Gamma_\phi}{\Delta Y^2} A(|P_{i,j-1/2}^{n+1}|) + \frac{\Delta\tau}{\Delta Y}[[V_{i,j-1/2}^{n+1}, 0]] \\
a_{i,j+1}^{n+1} &= \frac{\Delta\tau\Gamma_\phi}{\Delta Y^2} A(|P_{i,j+1/2}^{n+1}|) + \frac{\Delta\tau}{\Delta Y}[[-V_{i,j+1/2}^{n+1}, 0]] \\
a_{i,j}^{n+1} &= 2 + a_{i,j-1}^{n+1} + a_{i,j+1}^{n+1} \\
b^{n+1/2} &= 2\phi_{i,j}^{n+1/2} + \frac{\Delta\tau\Gamma_\phi}{\Delta X^2}\{A(|P_{i+1/2,j}^{n+1/2}|)(\phi_{i+1,j}^{n+1/2} - \phi_{i,j}^{n+1/2}) + A(|P_{i-1/2,j}^{n+1/2}|)\cdot(\phi_{i-1,j}^{n+1/2} - \phi_{i,j}^{n+1/2})\} \\
&\quad + \frac{\Delta\tau}{\Delta X}\{[[-U_{i+1/2,j}^{n+1/2}, 0]](\phi_{i+1,j}^{n+1/2} - \phi_{i,j}^{n+1/2}) + [[U_{i-1/2,j}^{n+1/2}, 0]](\phi_{i-1,j}^{n+1/2} - \phi_{i,j}^{n+1/2})\} \\
&\quad + \Delta\tau\cdot S_\phi^{n+1/2}
\end{aligned}\right\}, \tag{17b}$$

where

$$\left.\begin{aligned}
U_{i\pm1/2,j} &= \frac{1}{2}(U_{i,j} + U_{i\pm1,j}) \\
V_{i,j\pm1/2} &= \frac{1}{2}(U_{i,j} + U_{i,j\pm1}) \\
U_{i,j}^{n+1/2} &= \frac{1}{2}(U_{i,j}^n + U_{i,j}^{n+1})
\end{aligned}\right\}, \tag{18}$$

$$\left.\begin{aligned}
P_{i\pm1/2,j} &= \frac{\Delta X}{2\Gamma_\phi}(U_{i,j} + U_{i\pm1,j}) \\
P_{i,j\pm1/2} &= \frac{\Delta Y}{2\Gamma_\phi}(V_{i,j} + V_{i,j\pm1})
\end{aligned}\right\}. \tag{19}$$

The function $A(|P|)$ in Equation (17) is given by the following expression [10]

$$A(|P|) = [[0, (1 - 0.1|P|)^5]], \tag{20}$$

where the operator $[[a, b]]$ indicates the greater of a and b.

To complete the discretization process, the flow kinematics equation (9) is discretized using the central difference scheme. The final form of the equation becomes

$$\Psi_{i,j}^{n+1} = \frac{(\Delta Y)^2}{2[(\Delta X)^2 + (\Delta Y)^2]}(\Psi_{i+1,j}^{n+1} + \Psi_{i-1,j}^{n+1}) + \frac{(\Delta X)^2}{2[(\Delta X)^2 + (\Delta Y)^2]}(\Psi_{i,j+1}^{n+1} + \Psi_{i,j-1}^{n+1}) + \frac{(\Delta X \Delta Y)^2}{2[(\Delta X)^2 + (\Delta Y)^2]}\Omega_{i,j}^{n+1}. \tag{21}$$

Once $\Psi_{i,j}^{n+1}$ is calculated, $U_{i,j}^{n+1}$ and $V_{i,j}^{n+1}$ are determined as follows

$$\left.\begin{aligned} U_{i,j}^{n+1} &= \frac{1}{2\Delta Y}(\Psi_{i,j+1}^{n+1} - \Psi_{i,j-1}^{n+1}) \\ V_{i,j}^{n+1} &= \frac{1}{2\Delta X}(\Psi_{i-1,j}^{n+1} - \Psi_{i+1,j}^{n+1}) \end{aligned}\right\}. \tag{22a}$$

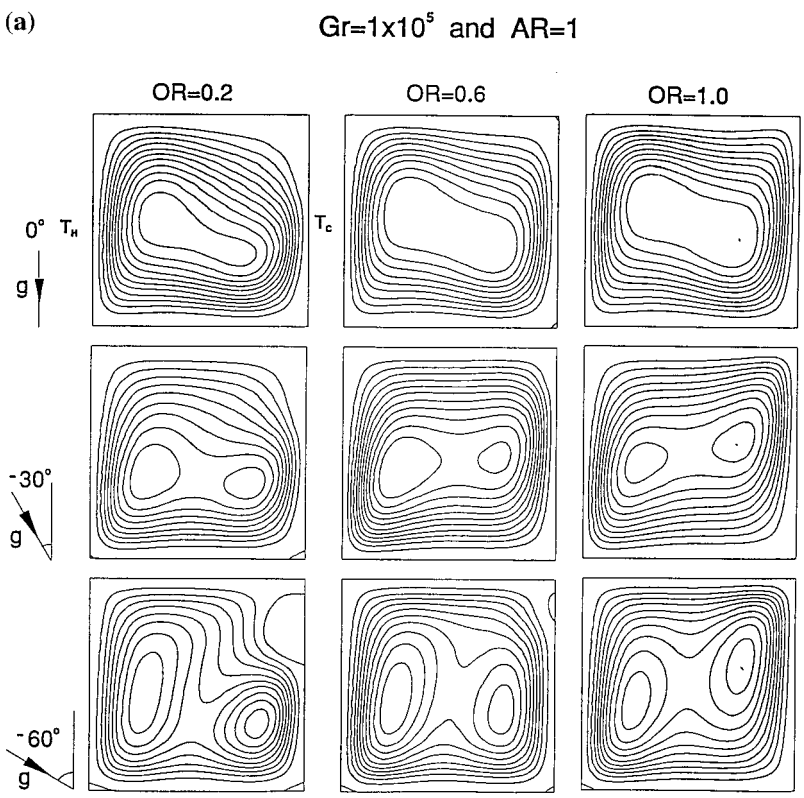

Figure 4. (a) Flow patterns for partially/fully cooled tilted cavities at $Gr = 1 \times 10^5$ and $AR = 1$. (b) Flow patterns for partially/fully cooled tilted cavities at $Gr = 1 \times 10^5$ and $AR = 1.33$. (c) Flow patterns for partially/fully cooled tilted cavities at $Gr = 1 \times 10^7$ and $AR = 2$. (d) Flow patterns for partially/fully cooled tilted cavities at $Gr = 1 \times 10^5$ and $AR = 4$.

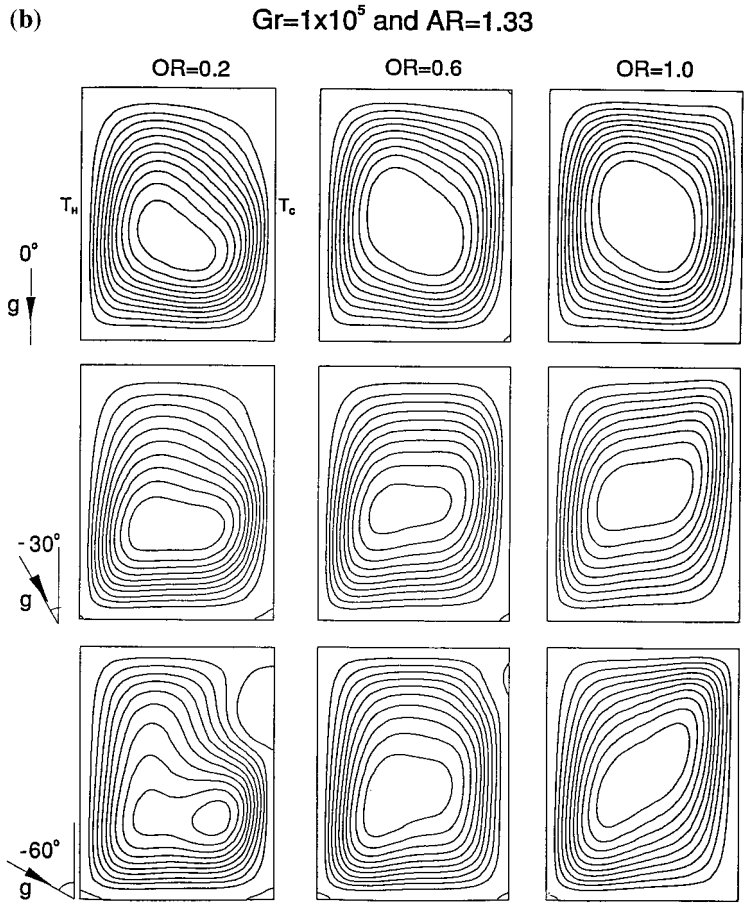

Figure 4 (*Continued*)

The vorticity on the boundaries is computed according to the following expressions

$$\text{at } Y=0 \qquad \Omega_{i,1}=\frac{(-4U_{i,2}^{n+1}+U_{i,3}^{n+1})}{2\Delta Y}, \tag{22b}$$

$$\text{at } Y=1 \qquad \Omega_{i,N}=\frac{(4U_{i,j-1}^{n+1}-U_{i,j-2}^{n+1})}{2\Delta Y}, \tag{22c}$$

$$\text{at } X=0 \qquad \Omega_{i,j}=\frac{(4V_{2,j}^{n+1}-V_{3,j}^{n+1})}{2\Delta X}, \tag{22d}$$

$$\text{at } X=B/H \qquad \Omega_{M,j}=\frac{(-4V_{M-1,j}^{n+1}+V_{M-2,j}^{n+1})}{2\Delta X}, \tag{22e}$$

where N and M are the total number of grid points.

In order to solve for the unknowns Ω and θ, the values of U^{n+1} and V^{n+1} must be known. They are not known, therefore, an iterative procedure is followed. For each iteration, the line tridiagonal matrix algorithm (see Richtmyer and Morton [12]) solves the linearized equations sequentially for θ and Ω. The value of $(\Omega_{i,j}^{n+1})^k$ is used in solving the kinematics equation which

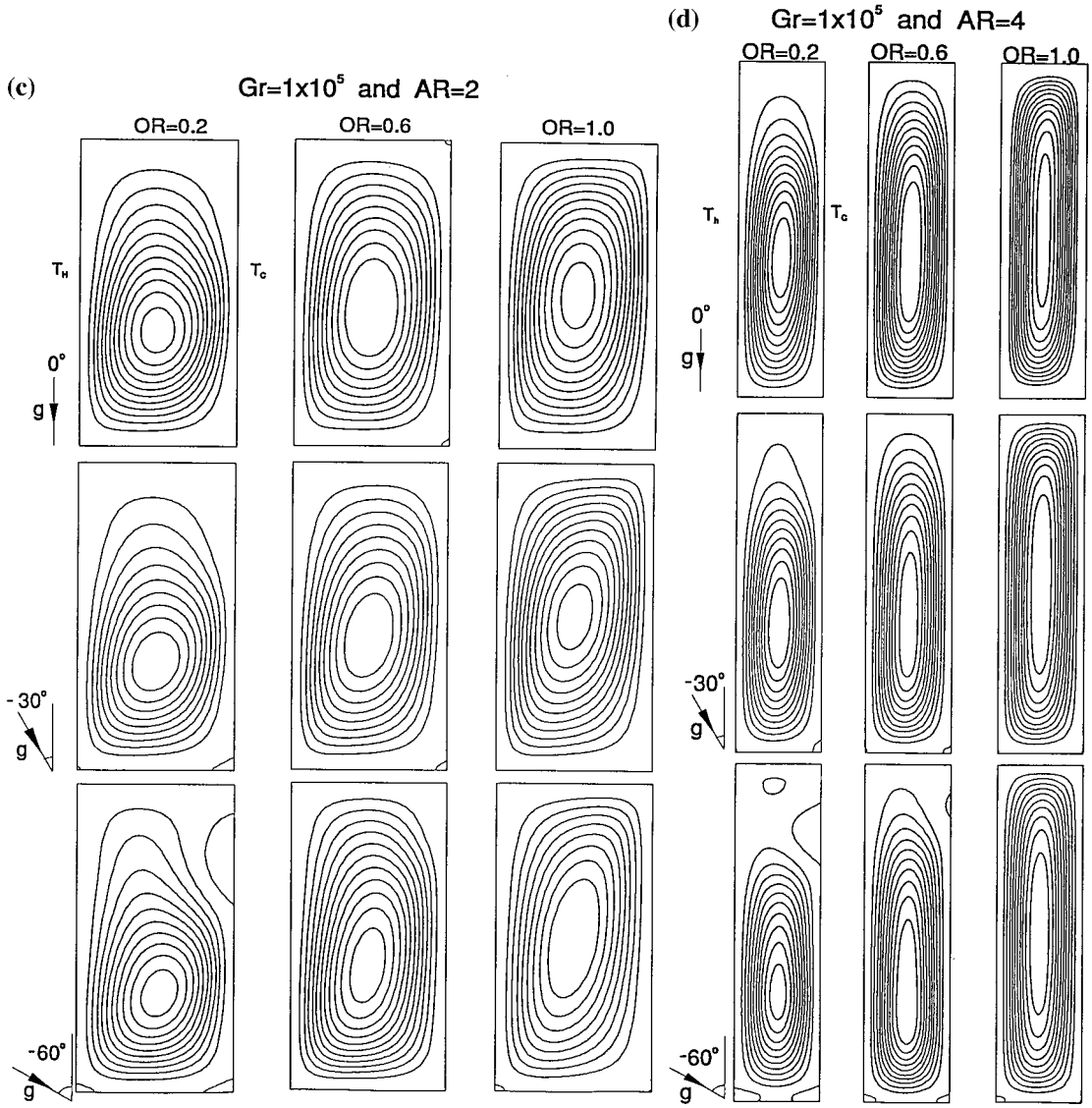

Figure 4 (*Continued*)

governs the Ψ distribution. The superscript k refers to the iteration number. The Ψ equation is solved by successive overrelaxation using the following expression

$$(\Psi_{i,j}^{n+1})^{m+1} = (1-\lambda)(\Psi_{i,j}^{n+1})^{m} + \frac{\lambda}{2[(\Delta X)^2+(\Delta Y)^2]}[(\Delta X)^2(\Psi_{i,j+1}^{n+1}+\Psi_{i,j-1}^{n+1})^{m} + (\Delta Y)^2(\Psi_{i+1,j}^{n+1}+\Psi_{i-1,j}^{n+1})^{m} + (\Delta X \Delta Y)^2(\Omega_{i,j}^{n+1})^{k}], \quad (23)$$

where λ is an overrelaxation factor. The following FITS [9] numerical procedure solves the kinetics and the kinematics of the problem.

1. Select a coarse grid. An 11×11 grid is a good start in many cases.
2. Use trial and error procedure to select the corresponding largest possible time step.
3. Assume initial solutions for U^n, V^n, θ^n and Ω^n, or get these values at an earlier time level.
4. As a first trial, assign the values of U^n and V^n to U^{n+1} and V^{n+1}.
5. Use U^{n+1} and V^{n+1} to calculate θ^{n+1} using Equations (15) and (16) with ϕ to stand for θ.
6. Use the values of U^{n+1}, V^{n+1} and θ^{n+1} to determine Ω^{n+1} from Equations (15) and (16).
7. Solve Equation (21) to determine Ψ^{n+1}.
8. Determine new values of U^{n+1} and U^{n+1} from the values of Ψ^{n+1} using central difference given by Equation (22).
9. Use the new values of U^{n+1} and V^{n+1} to repeat steps 5–8. Check convergence of Ω^{n+1} and θ^{n+1}, if not converged repeat steps 5–8.
10. Repeat steps 4–9 for advancing time levels until steady state convergence is achieved.
11. Repeat steps 2–10 successively for refined grids.
12. Check the solution grid independence by comparing the results obtained from two successive grids and repeat step 11 if necessary.

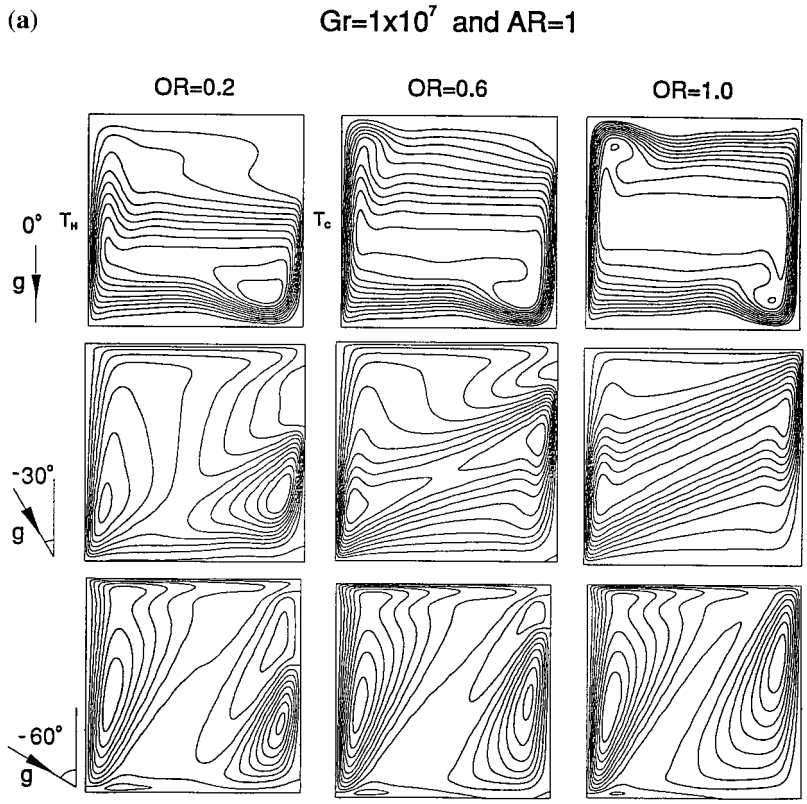

Figure 5. (a) Flow patterns for partially/fully cooled tilted cavities at $Gr = 1 \times 10^7$ and $AR = 1$. (b) Flow patterns for partially/fully cooled tilted cavities at $Gr = 1 \times 10^7$ and $AR = 1.33$. (c) Flow patterns for partially/fully cooled tilted cavities at $Gr = 1 \times 10^7$ and $AR = 2$. (d) Flow patterns for partially/fully cooled tilted cavities at $Gr = 1 \times 10^7$ and $AR = 4$.

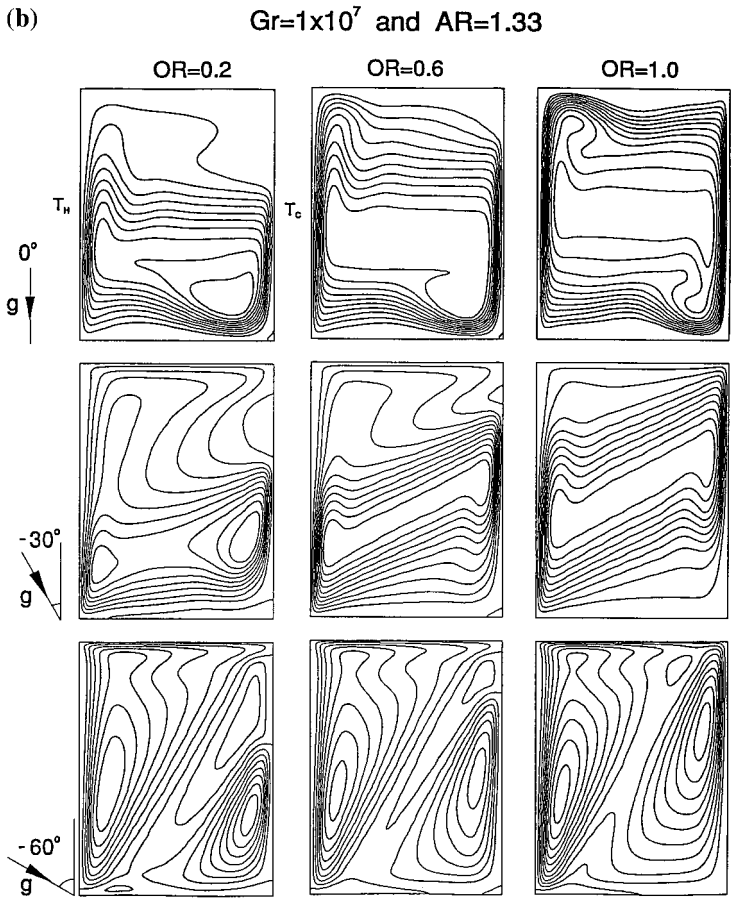

Figure 5 (*Continued*)

3. VALIDATION OF THE COMPUTER CODE

The computer code which employs the FITS algorithm has been validated for natural convection in a differentially heated tilted square cavity. As seen in Figure 3, the present predictions for $Ra = 10^6$ and range in tilt angle ($-90° \leq \alpha \leq 0°$) are in good agreement with published data and solutions [13–16].

3.1. Grid refinement

Many numerical experiments of various mesh sizes have been performed using the FITS algorithm to determine the best compromise between accuracy of the results and minimizing computer time. Based on these results, a mesh size of 40×40 has been adopted for all the cases completed in the present study. As shown previously by El-Refaee *et al.* [9], further increase of the mesh size did not significantly change the final steady state results for $10^5 \leq Ra \leq 10^7$. The steady state solution is assumed to be converged when the variation of the Nusselt number between two consecutive time steps is $< 0.1\%$. Computations were performed on the VAX 9000/420 super-mini (vector processing) computer.

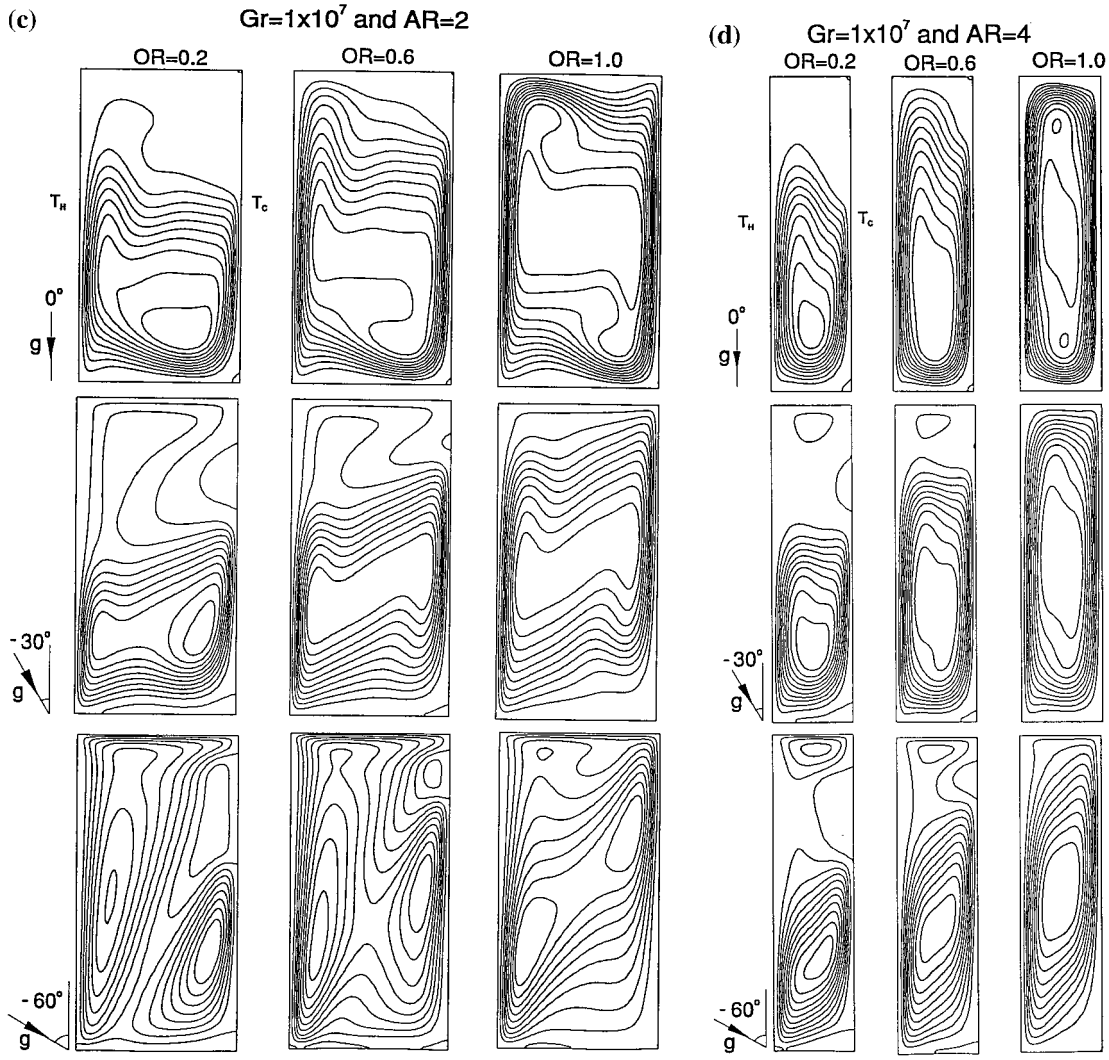

Figure 5 (*Continued*)

4. RESULTS AND DISCUSSION

Solutions are obtained for air ($Pr = 0.7$) at $Gr_H = 10^5$ and 10^7 with cavities (Figure 2) having: $AR = H/B = 1$, 1.33, 2 and 4; $OR = a/H = 0.2$, 0.6 and 1.0; and $\alpha = 0°$, $-30°$, $-60°$ and $-90°$, where $\alpha = -90°$ represents a tilted cavity with the hot wall facing downward.

4.1. Flow pattern

The flow patterns inside cavities at different values of AR, OR and α are given in Figure 4(a)–(d) and Figure 5(a)–(d) for $Gr_H = 10^5$ and 10^7, respectively. Considering a flow with $Gr_H = 10^5$, $AR = 1$, $OR = 1$ and $\alpha = 0°$, it is evident in Figure 4(a) that the two major inner vortices control the flow in the cavity. One of these vortices (vortex Ω_h) is generated by the hot wall and the other (vortex Ω_c) is generated by the cold wall. The locations of these two vortices

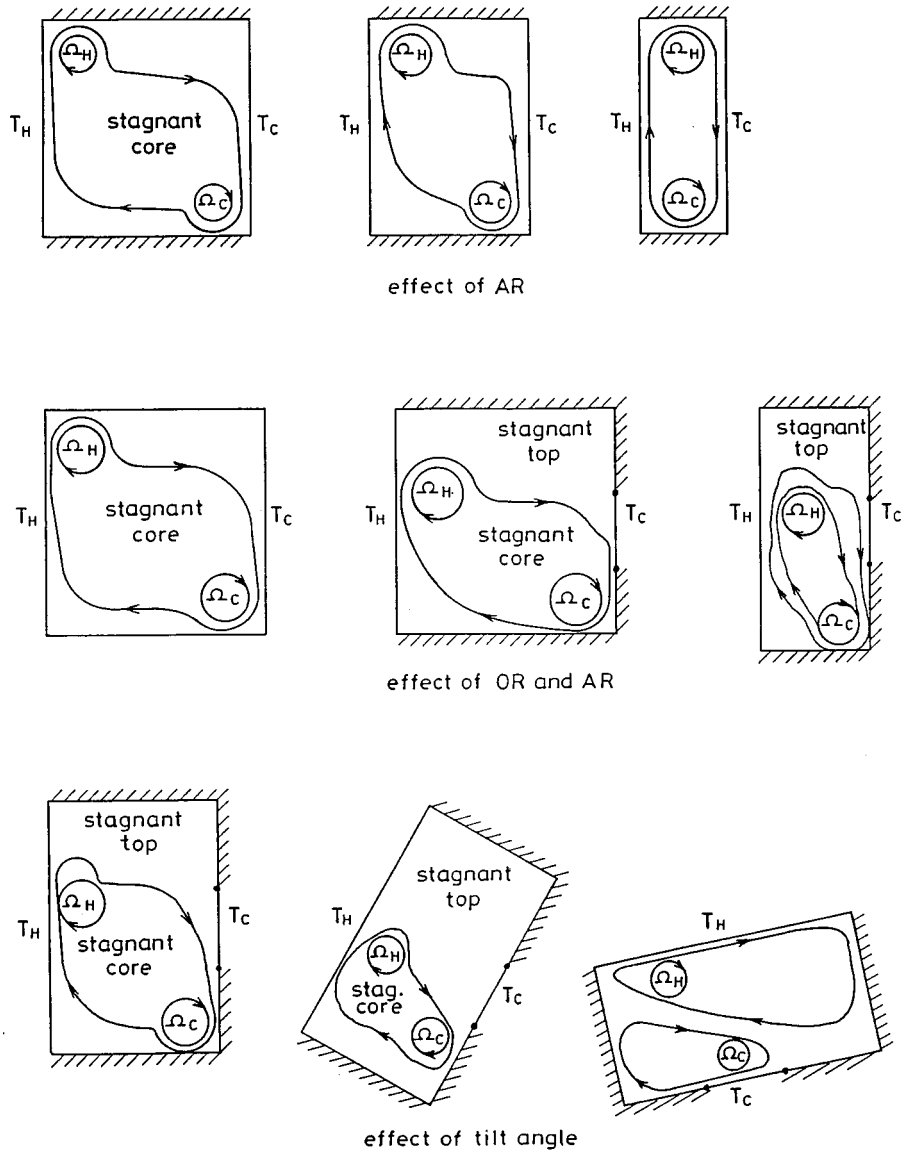

Figure 6. Effect of *AR*, *OR* and α on flow pattern.

are strongly dependent on the values of *OR* and *AR*. As α decreases from 0° to $-90°$, vortex Ω_c moves up along the cold wall and vortex Ω_h moves down along the hot wall. On the other hand, as *OR* decreases for a constant α, Ω_c moves down along the cold wall while the location of Ω_h is approximately unaffected. The span between the centers of the vortices Ω_c and Ω_h decrease as *AR* increases, until the two vortices merge at high values of *AR* (see Figure 4(a)–(d)).

As *Gr* increases from 10^5 to 10^7 for a vertical fully cooled square cavity (i.e. $AR = 1$, $\alpha = 0°$ and $OR = 1$), the center of vortex Ω_h moves towards the edge of the hot wall at the top, while

the center of vortex Ω_c moves towards the edge of the cold wall at the bottom. Therefore, the flow accelerations near the hot and cold walls are increased and the boundary layers near the hot and cold walls become thinner with increasing *Gr*. This mechanism, in turn, increases the horizontal distance between the centers of the two vortices, and finally the core region becomes stagnant (see Figure 4(a) Figure 5(a)).

The effect of α on the dynamics of the vortices inside the cavity is almost the same for both values of *Gr* (10^5 and 10^7). As α decreases from 0° to $-90°$ (clockwise rotation), Ω_h moves down along the hot walls whereas Ω_c moves up along the cold walls (Figure 5(a)). This behavior in turn reduces the vertical height of the stagnant core. The stagnant core vanishes when the tilt angle α is decreased below its critical value α^* (Figure 5(a)). The critical angle α^* is defined as the tilt angle when Ω_c moves above Ω_h.

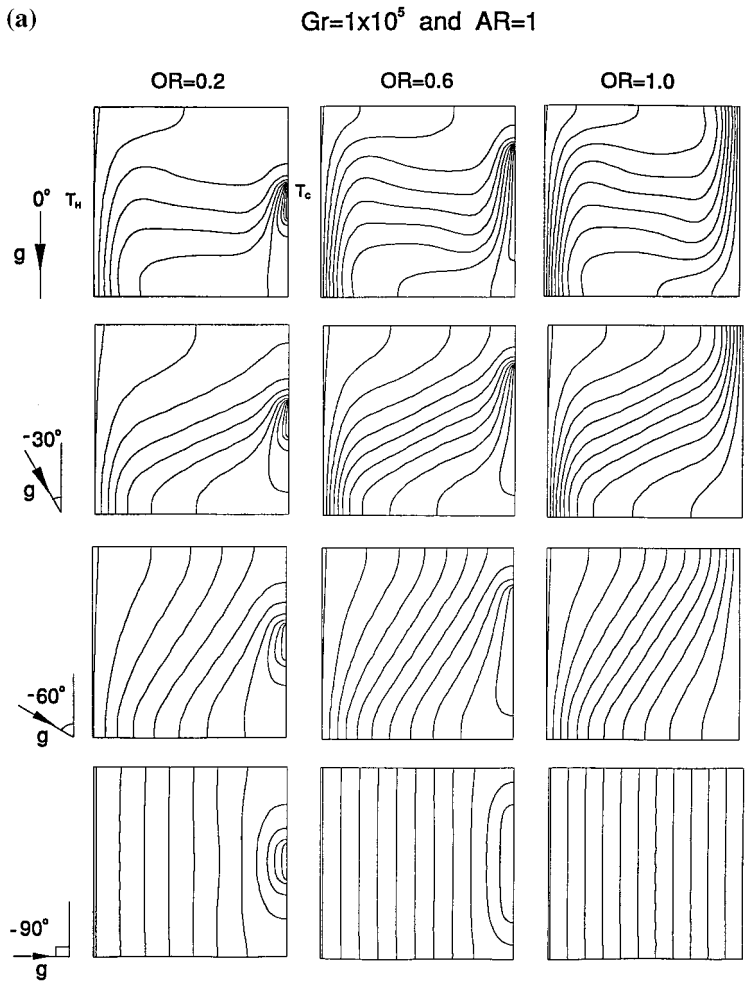

Figure 7. (a) Isotherm contours for partially/fully cooled tilted cavities at $Gr = 1 \times 10^5$ and $AR = 1$. (b) Isotherm contours for partially/fully cooled tilted cavities at $Gr = 1 \times 10^5$ and $AR = 1.33$. (c) Isotherm contours for partially/fully cooled tilted cavities at $Gr = 1 \times 10^5$ and $AR = 2$. (d) Isotherm contours for partially/fully cooled tilted cavities at $Gr = 1 \times 10^5$ and $AR = 4$.

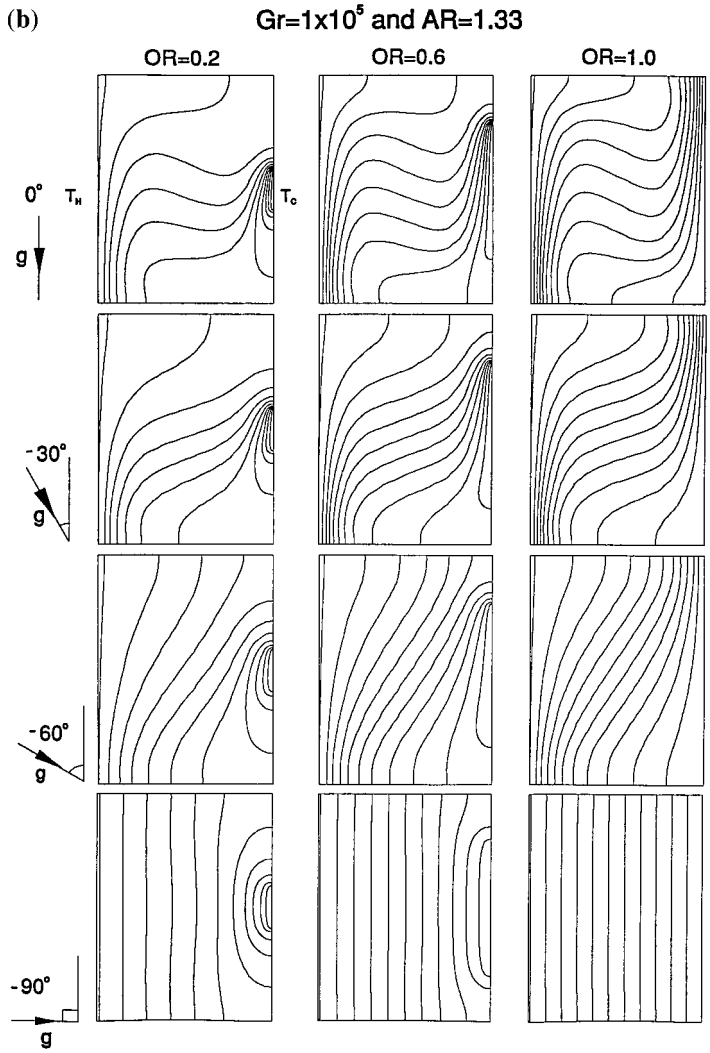

Figure 7 (*Continued*)

A significant effect of the sink–source area ratio OR on the dynamics of the vortices is also predicted in the present work for $Gr_H = 10^7$. The effect of decreasing OR restricts the maximum height that Ω_c can reach, which is the upper edge of the cold wall. When $AR = 1$, a stagnant zone forms near the top of the cavity and the vertical height of this zone increases with the decrease of OR. Moreover, as OR decreases, the stagnant core moves closer to the lower part of the cavity and its vertical height decreases.

As evident in the figures, the combined contributions of tilting the cavity and decreasing OR assist in the diminishing of the vertical height of the stagnant core. Therefore, the critical tilt angle gets closer to the vertical position as OR decreases. In the same time, the aspect ratio AR increases, and the critical tilt angle (at $Gr_H = 10^7$) decreases. Similarly, the vertical height of the stagnant core at a given tilt angle increases as AR increases. When this distance becomes small enough, the two vortices merge to form one larger vortex. The same behavior has been observed earlier for $Gr_H = 10^5$.

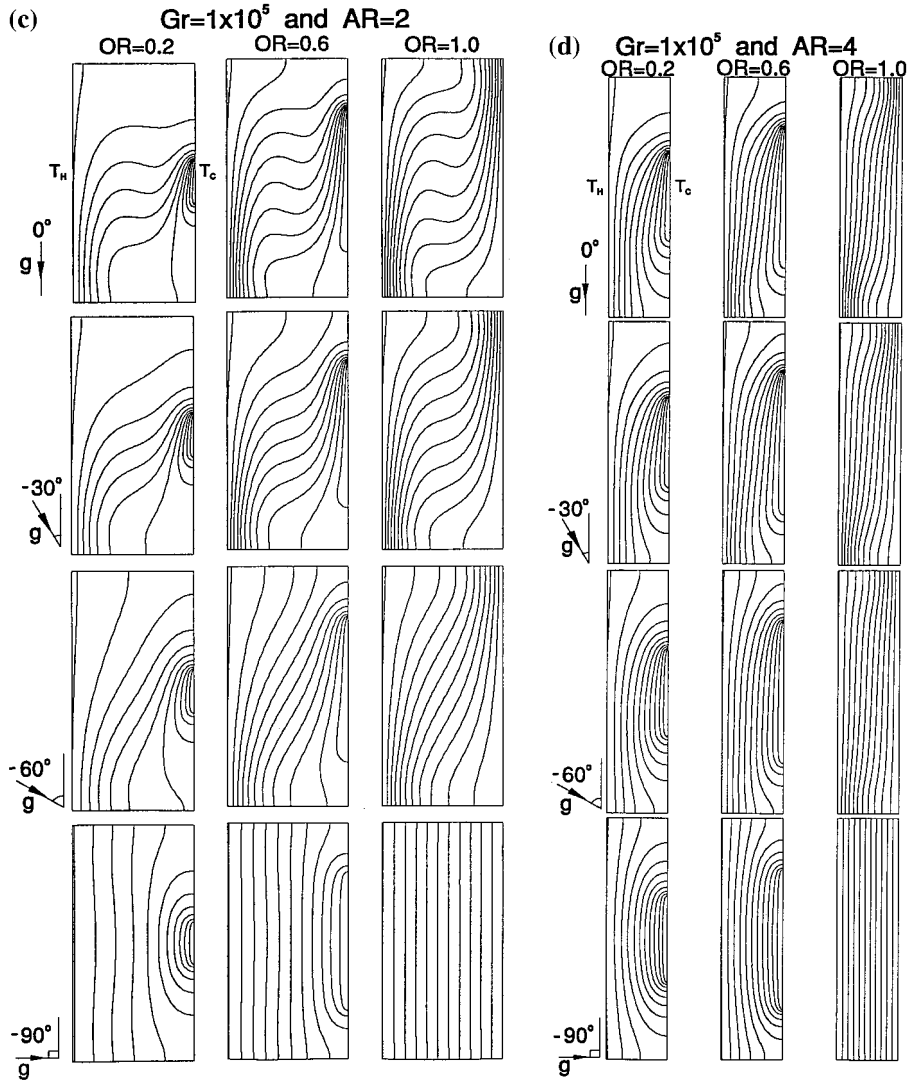

Figure 7 (*Continued*)

Figure 6 depicts a summary of the effects of changing AR, OR and α on the flow pattern in the cavity as illustrated above.

4.2. Isotherm contours

The steepest temperature gradient occurs near the hot and cold walls, elsewhere, most of the fluid in the cavity is stratified (see Figures 7 and 8). With the increase in Gr_H, the thermal boundary layers near the heated and cooled walls become thinner, and thus, stratification of the fluid in the cavities becomes more pronounced. Decreasing OR and/or decreasing the tilt angle from 0° to $-90°$ encourages stratification. When AR increases, the tendency for stratification of the cavity fluid diminishes, i.e. vertical cavities with $AR = 4$ have no stratifica-

tion at all (see Figure 7(d)). However, increases in Gr_H (see Figure 8(d)) diminish this effect. Also at high AR, stratification takes place at the upper part of the cavity upon decreasing OR.

4.3. Cavity average Nusselt number

The local heat transfer coefficient for the convective rate of heat transfer between heated and cooled walls is defined as follows

$$h = -\frac{k}{B}\left(\frac{\mathrm{d}\theta}{\mathrm{d}X}\right)_{X=0}. \tag{24}$$

The cavity average Nusselt number is defined by the following expression

$$\bar{N}u_B = \frac{\bar{h}B}{k} = -\frac{1}{AR}\int_0^1 \left(\frac{\mathrm{d}\theta}{\mathrm{d}X}\right)_{X=0} \mathrm{d}Y. \tag{25}$$

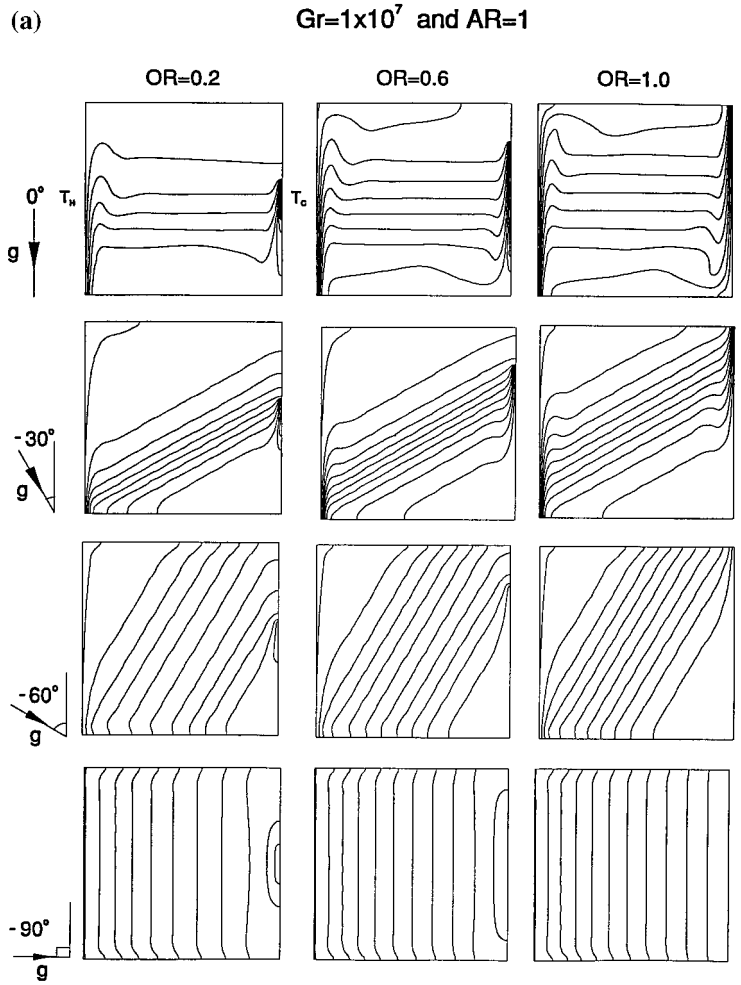

Figure 8. (a) Isotherm contours for partially/fully cooled tilted cavities at $Gr = 1 \times 10^7$ and $AR = 1$. (b) Isotherm contours for partially/fully cooled tilted cavities at $Gr = 1 \times 10^7$ and $AR = 1.33$. (c) Isotherm contours for partially/fully cooled tilted cavities at $Gr = 1 \times 10^7$ and $AR = 2$. (d) Isotherm contours for partially/fully cooled tilted cavities at $Gr = 1 \times 10^7$ and $AR = 4$.

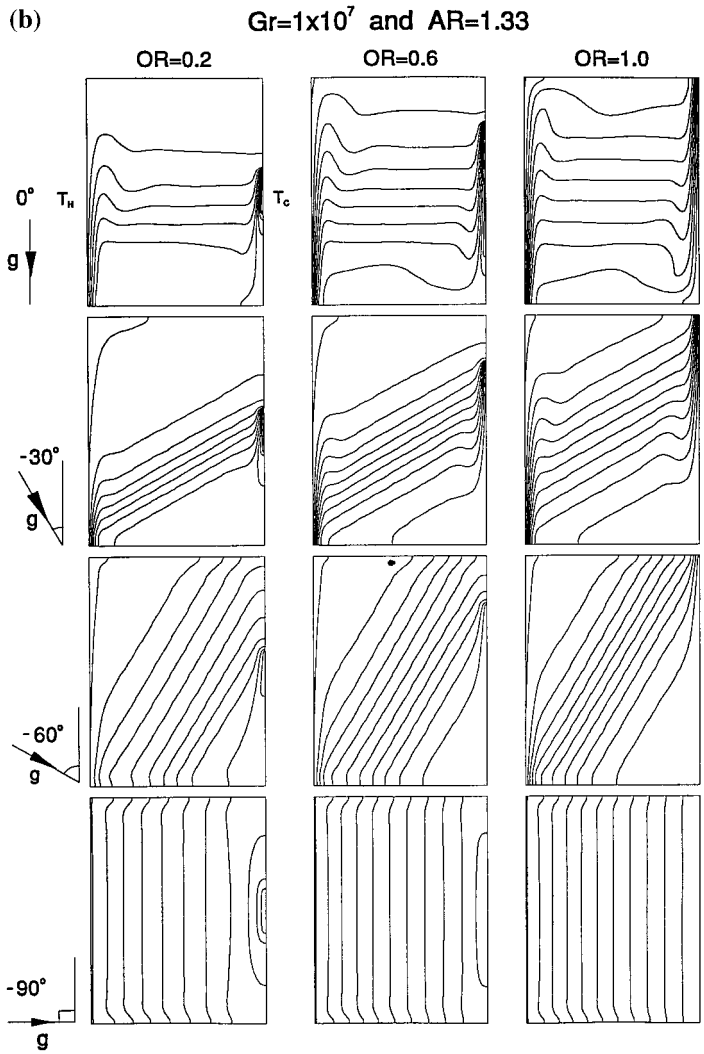

Figure 8 (*Continued*)

Figure 9(a,b) show the variation of $\bar{N}u_B$ at different values of AR and OR for cavities with $Gr_H = 10^5$ and 10^7, respectively. As shown in the figures, vertical cavities always have higher $\bar{N}u_B$ than tilted ones (hot wall facing downward). As the tilt angle α decreases, the buoyancy effects become stronger and the natural convection from hot to cold wall is suppressed until $\alpha = -90°$, when heat transfer from hot to cold wall is carried out fully by conduction, i.e. $\bar{N}u_B$ tends to 1.

On the other hand, the value of $\bar{N}u_B$ decreases with the decrease of OR, since the area of the heat sink per unit area of the heat source is decreased. This trend is always true regardless of the value of Gr_H, AR, or α. However, this effect of OR diminishes as α approaches $-90°$. In a horizontal cavity, i.e. as OR is decreased, the resistance to heat conduction from source to sink is increased, which in turn decreases the average Nusselt number $\bar{N}u_B$ below unity (see Figure 9(a) at $OR = 0.2$).

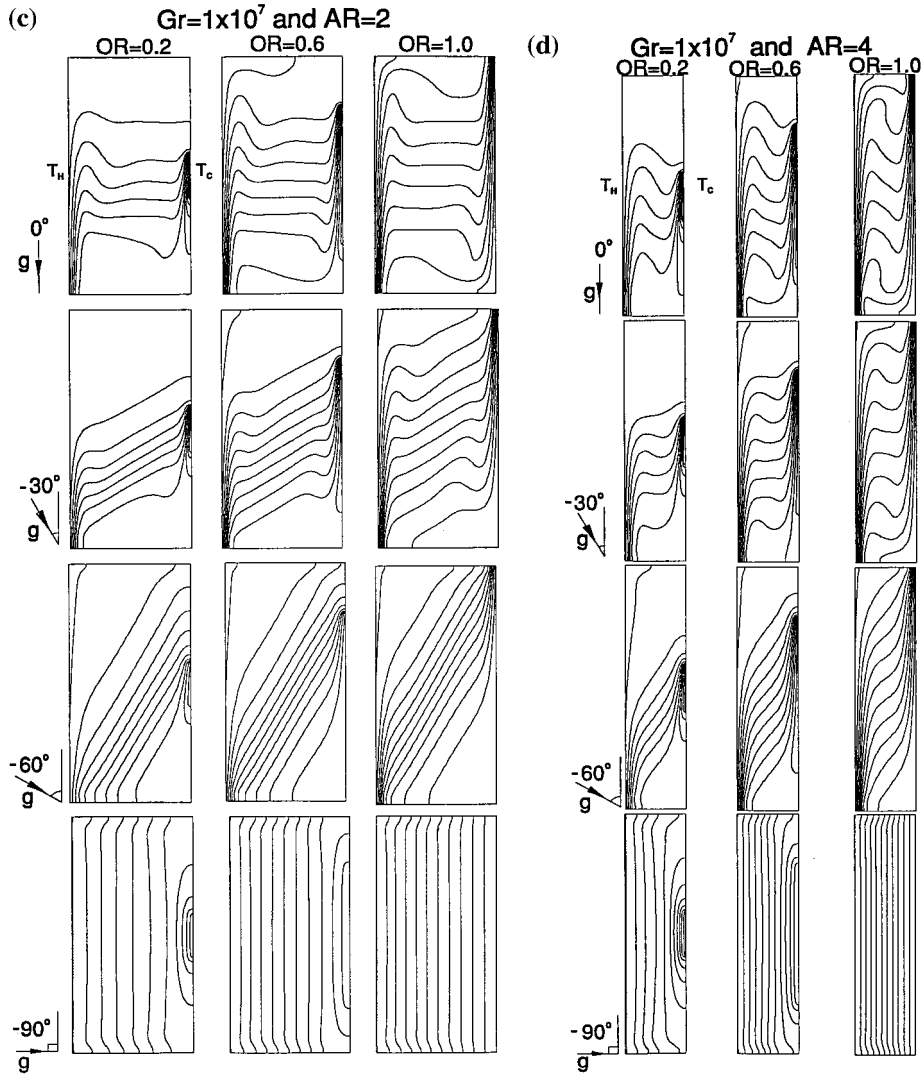

Figure 8 (*Continued*)

As expected, the increase of AR decreases the value of $\bar{N}u_B$. The reason is obvious: as the width of the cavity per unit height of the hot wall is decreased, the vertical boundary layers of the hot and cold walls are in better thermal contact with each other, which reduces the degree of heating and cooling the hot and cold wall boundary layers, respectively, thus lowering the overall Nusselt number. Once again, the effect of an increasing AR on $\bar{N}u_B$ diminishes as α approaches $-90°$.

In vertical cavities, $\alpha = 0°$, increasing Gr_H from 10^5 to 10^7 improves the value of $\bar{N}u_B$ by an order of three to four times, regardless of the values of OR and AR. Again, this effect becomes less pronounced as α approaches $-90°$, when heat is transferred only by pure conduction and thus the value of Gr_H has no role in the mechanism of heat transfer.

5. CONCLUDING REMARKS

The main conclusions that are drawn from the study are

1. The results have shown a significant effect of the geometric parameters of the cavity (AR, α, OR) on the average Nusselt number. The effect is greater for higher Rayleigh number. At $Ra = 10^7$, the average Nusselt number of a vertical fully cooled square cavity is approximately 350% greater than that at $Ra = 10^5$.
2. The average Nusselt numbers drop sharply as the tilt angle decreases from 0° to $-90°$ (cavity heated from the top). However, this drop gets smaller as the source–sink ratio (OR) is decreased (Figure 9(a)). The slope of the $\bar{N}u_B$–α variation is considerably decreased when α is decreased beyond its critical value α^*. The Nusselt number reaches unity for horizontal cavities ($\alpha = -90°$) irrespective of the values of the aspect ratio AR, and the source–sink ratio OR. This may be attributed to the full domination of the conduction process (vanishing of the good mixing stagnant core) as the tilt angle α decreases to its minimum value.

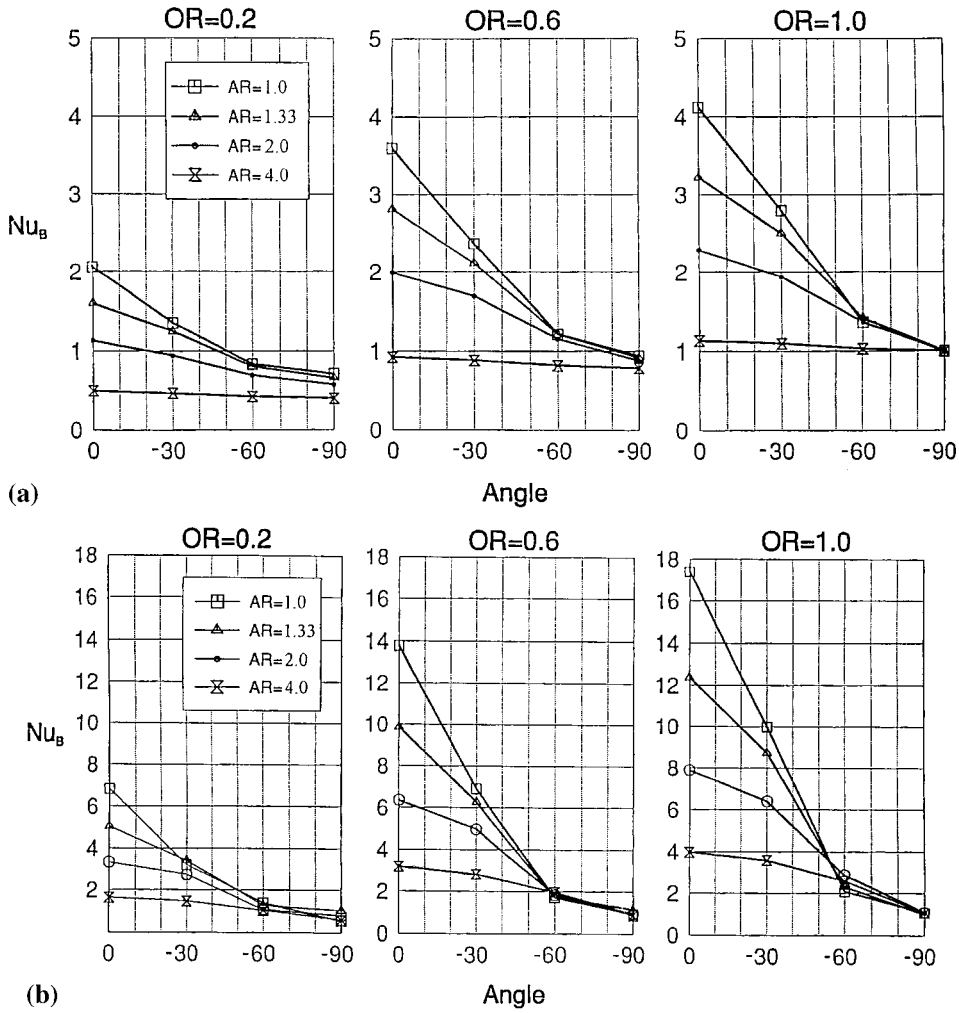

Figure 9. (a) Dependence of cavity Nusselt number on tilt angle, aspect ratio and opening ratio at $Gr = 1 \times 10^5$. (b) Dependence of cavity Nusselt number on tilt angle, aspect ratio and opening ratio at $Gr = 1 \times 10^7$.

3. At higher values of aspect ratio ($AR = 4$), the heat transfer rates for all angles tend to approach unity irrespective of OR as the conduction limit is approached (Figure 7). However, the effect of AR becomes more significant at smaller values of OR ($OR = 0.2$) (Figure 9(a,b)).
4. The rate of heat transfer reaches its maximum value when the cavity is vertical with unity AR and unity OR.
5. The combined effect of aspect ratio and tilt angle on the rate of heat transfer becomes less significant for cavities with smaller OR.

APPENDIX A. NOMENCLATURE

$a_{i,j}$	coefficient of finite difference equation at point (i, j) in a grid
A	function of power law
AR	aspect ratio, $AR = H/B$
b	right-hand-side of finite difference equation
B	cavity width
c_p	specific heat at constant pressure
g	gravitational acceleration
Gr	Grashof number
h	heat transfer coefficient
H	cavity height (characteristic length)
k	thermal conductivity of the fluid in the cavity
OR	opening ratio
p	pressure
Pr	Prandtl number of the fluid in the cavity
Ra	Rayleigh number
S_ϕ	source term, Equation (13)
t	time
T	temperature
u	velocity component in x-co-ordinate direction
U	dimensionless velocity component in x-co-ordinate direction
v	velocity component in y-co-ordinate direction
V	dimensionless velocity component in y-co-ordinate direction
x, y	Cartesian co-ordinates
X	dimensionless x-co-ordinate distance
Y	dimensionless y-co-ordinate distance

Greek letters

α	cavity tilt angle
β	coefficient of thermal expansion
Γ_ϕ,	diffusion coefficient, Equation (13)
θ	dimensionless temperature
υ	kinematic diffusivity
ρ_o	density at reference temperature
τ	dimensionless time
λ	overrelaxation factor
ϕ	general dependent variable, Equation (13)
Ψ	dimensionless streamfunction
ψ	streamfunction

Ω dimensionless velocity
ω vorticity

Subscripts

c cold
h hot
i X-location of a grid point
j Y-location of a grid point

Superscript

k iteration number for solving Ω and θ equations
m iteration number for solving ψ equation
n time level

REFERENCES

1. S. Ostrach, 'Natural convection in enclosures', *Trans. ASME J. Heat Transfer*, **110**, 1175–1190 (1981).
2. R.J. Krane and J. Jessee, 'Some detailed field measurements for a natural convection flow in a vertical square enclosure', *Proc. 1st ASME-JSHE Thermal Engineering Joint Conf.*, **1**, 323–329 (1983).
3. G. Barakos, E. Mitsoulis and D. Assimacopoulos, 'Natural convection flow in a square cavity revisited: laminar and turbulent models with wall functions', *Int. j. numer. methods fluids*, **18**, 695–719 (1994).
4. N.C. Markatos and K.C. Pericleous, 'Laminar and turbulent natural convection in an enclosed cavity', *Int. J. Heat Mass Transfer*, **27**, 772–775 (1984).
5. R.A.W. Henkes, F.F. van der Vlugt and C.J. Hoogendoorn, 'Natural convection flow in a square cavity calculated with low-Reynolds-number turbulence model', *Int. J. Heat Mass Transfer*, **34**, 1543–1557 (1991).
6. P.H. Oosthuizen and J.T. Paul, 'Free convective flow in an inclined square cavity with a partially heated wall', *ASME HTD, Heat Transfer in Convective Flows*, National Heat Transfer Conference, Philadelphia, 1989, p. 107.
7. M. Hasnaoui, E. Bilgen and P. Vasseur, 'Natural convection heat transfer in rectangular cavities partially heated from below', *J. Thermophys. Heat Transfer*, **6**, 255–264 (1992).
8. B.L. Turner and R.D. Flack, 'The experimental measurement of natural convective heat transfer in rectangular enclosures with concentrated energy sources', *Trans. ASME, J. Heat Transfer*, **102**, 236–241 (1980).
9. M.M. El-Refaee, M.M. Elsayed, N.M. Al-Najem and I.E. Megahid, 'Steady-state solutions of buoyancy-assisted internal flows using a fast false implicit transient scheme (FITS)', *Int. J. Heat Fluid Flow*, **6**, 3–23 (1995).
10. S.V. Patankar, *Numerical Heat and Fluid Flow*, *Hemisphere*, New York, 1980.
11. R.H. Pletcher, W.J. Minkowycz, E.M. Sparrow and G.E. Schneider, 'Overview of basic numerical methods', *Handbook of Numerical Heat Transfer*, Wiley, New York 1988.
12. R.D. Richtmyer and K.W. Morton, *Difference Methods for Initial-Value Problems*, 2nd edn., Wiley, New York, 1967.
13. R.A. Kupyer, T.H. Van Der Meer, C.J. Hoogendoorn and R.A.W.M. Henkes, 'Numerical study of laminar and turbulent natural convection in an inclined square cavity', *Int. J. Heat Mass Transfer*, **36**, 2899–2911 (1993).
14. Z.Y. Zhong, K.T. Yang and J.R. Lloyd, 'Variable property effects in laminar natural convection in a square enclosure', *Trans. ASME J. Heat Transfer*, **107**, 133–138 (1985).
15. I. Catton, P.S. Ayyaswamy and R.M. Clever, 'Natural convection flow in a finite, rectangular slot arbitrarily oriented with respect to the gravity vector', *Int. J. Heat Mass Transfer*, **17**, 173–184 (1974).
16. F.J. Hamady, J.R. Lloyd, K.T. Yang and H.Q. Yang, 'A study of natural convection in a rotating enclosure', *Trans. ASME J. Heat Transfer*, **116**, 136–143 (1994).
17. D. Kuhn and P.H. Oosthuizen, 'Unsteady natural convection in a partially heated rectangular cavity', *Trans. ASME J. Heat Transfer*, **109**, 798–801 (1987).
18. P.H. Oosthuizen and J.T. Paul, 'Free convection in a square cavity with a partially heated wall and a cooled top', *J. Thermophys.*, **5**, 583–588 (1991).
19. M. Keyhani, V. Prasad and R. Cox, 'An experimental study of natural convection in a vertical cavity with discrete heat sources', *Trans. ASME J. Heat Transfer*, **110**, 616–624 (1988).
20. A. Hadim and M. Ramot, 'Natural convection in an enclosure with discrete heat sources on the vertical walls', ASME Winter Annual Meeting, *Paper no. 93-WA/EEP-26*, New Orleans (1993).

